Solar Energy Materials and Solar Cells 180 (2018) 271–279

Contents lists available at ScienceDirect

Solar Energy Materials and Solar Cells

journal homepage: www.elsevier.com/locate/solmat

Experimental investigation and modeling of the thermal behavior of a solar PV module

M. Akhsassi, A. El Fathi, N. Erraissi, N. Aarich, A. Bennouna*, M. Raoufi, A. Outzourhit

LN2E (ex-LPSCM), Physics Department, Faculty of Science Semlalia, Cadi Ayyad University, Marrakech, Morocco

ARTICLE INFO

Keywords:
PV cells temperature
PV module temperature
Experimental measurements
Theoretical models
Comparative study

ABSTRACT

Photovoltaic (PV) cell/module/array temperature calculations are essential to accurately assess its electrical performance. In this paper, we developed and validated two new models, and then we focused on the comparison of ten theoretical models (including our models) with experimental measurements, based on the ambient temperature, the in-plane array irradiance with/without taking into account the wind speed. These models were used to determine the PV module temperature of a 7.2 kWp standalone photovoltaic power plant installed in Elkaria village (Province of Essaouira, Morocco). The results show that our model without wind yields the highest value of the correlation coefficient $R^2 = 96.7\%$ and the lowest value of the root mean square error RMSE = 1.6 °C among the models without wind. On the other hand, our model with wind gives the best statistical coefficients ($R^2 = 98.8\%$ and RMSE = 1.1 °C) compared to all models (with/without wind).

1. Introduction

In the development of the photovoltaic industrial market, there is an increasing demand for accurate models forecasting the energy yield. There are several parameters affecting the PV module efficiency. The first of these is the plane of the module irradiance, G_g, and the second one is the PV module temperature, T_m. The latter parameter is:

- in most cases, assumed as being the same as the cell temperature, T_c, [1],
- sometimes considered to be lower than T_c by about 3 °C for an irradiance of 1000 W/m^2, as in the work of King et al. [2], or treated in a different way [3].

The PV module temperature affects negatively its voltage and positively its current. The power temperature coefficient (β_{Pmp}) for crystalline silicon encapsulated solar cells is usually not measured but determined using a calculation procedure according to the IEC 60891 standard, and it is in the range of -0.52 to $-0.37\%\ °C^{-1}$ [4]. King et al. [2] showed that the efficiency of three PV modules technologies can decrease by up to 10% for the highest module temperatures.

The electrical parameters of PV modules are usually measured by the manufacturers at Standard Test Conditions (STC): an irradiance level of 1000 W/m^2, a cell temperature of 25 °C and an air mass AM = 1.5 spectrum. In fact, these conditions occur rarely on site since solar radiation of 1000 W/m^2 makes it difficult to have a cell temperature of 25 °C [4]. The normal operating cell temperature (NOCT), defined by IEC61215 [5] standard, is measured on an open rack-mounted module with an inclination of 45°, an irradiance level of 800 W/m^2, an ambient temperature of 20 °C and a wind speed of 1 m/s. The effect of different operational conditions (open-circuit, maximal power point, …) on the temperature of a PV module was found not to be negligible and is also dependent on the actual electrical efficiency [6]. The PV module temperature depends on several factors; incident solar radiation, ambient temperature, wind speed and direction, physical properties of the module materials, and mounting structure [2,7,8]. For free-standing modules, in a normal summer day in Germany with an irradiance of 800 W/m^2 and an ambient temperature of 20 °C, the common module temperature is around 42 °C [9], while during cloudy summer days in Central Europe, it can easily reach 60 °C. In extreme conditions, the PV module temperature can exceed 80 °C in Ouarzazate (Morocco) [10], where it is planned to install a 70 MWp photovoltaic power plant in the framework of the Moroccan Solar Plan (Noor IV project). In reference [10], the authors applied a standard NOCT model developed by Nolay [11] which is used in most simulation software to obtain the module temperature from ambient temperature and incident solar radiation, but ignores the effect of the wind. Muller [12] explained why NOCT based models do not explain temperature variations under specific conditions since, for instance, they do not take into account radiation heat losses from the front and rear module surfaces to sky and to ground, respectively. In the Lasnier et al. [13] developed an empirical correlation to obtain the polycrystalline silicon module temperature.

* Corresponding author.
E-mail address: sindibad@uca.ac.ma (A. Bennouna).

http://dx.doi.org/10.1016/j.solmat.2017.06.052
Received 19 March 2017; Received in revised form 20 June 2017; Accepted 26 June 2017
Available online 05 July 2017

However, this model does not taking account the effect of wind and the obtained empirical parameters cannot be used for other PV module technologies.

Several authors, such as, King et al. [2], Duffie and Beckman [14], Skoplaki et al. [15], Koehl et al. [16], Kurtz et al. [17], Mattei et al. [1], Barroso et al. [18] and Faiman et al. [7] developed thermal models for PV systems taking into account the wind effect on PV cell/module/array temperature calculations. Koehl et al. [6] reported a wind cooling effect of 15–20 °C for wind speeds of 10 m/s at a solar irradiance of about 1000 W/m^2.

The behavior of the PV module as a thermal mass has been described in the literature [19–23]. For non-steady-state conditions, the thermal time constant of encapsulated solar cells can reach 7 min [22], 15 min [23] or 10.5 min [19], depending on the wind speed.

In most PV systems, measured PV module temperature is not available. Hence, it is desirable to model physical relations between the PV module temperature, incoming irradiance, ambient temperature and, when available, wind speed. Even with a small impact for slow winds, the latter remains a pertinent factor that, when available, should be taken into account to calculate PV module temperatures. However, due to the difficulty of predicting winds, more accurate models ignoring wind speeds are necessary to forecast future PV systems yield within the framework of the Moroccan Solar Plan (MSP) [23,24]. For this reason, we decided to evaluate the accuracy of the module temperature models from onsite measurements:

- ignoring wind, considering plane of array irradiance, Gg and ambient temperature, Ta,
- considering the wind speed v.
- The objective of the present work is to:
- propose and validate two new models that calculate the PV module temperature with/without wind,
- compare the results of our models and of eight existing models (with/without wind), with onsite measurements.

Results of this paper are indented to be used in the framework of the "*Propre.ma*" project whose main goal consists on constructing grid-connected photovoltaic yield maps for all Morocco with ground calibration using identical plants installed in partner institutions located in 20 different Moroccan cities.

2. Experimental setup

2.1. Description of the photovoltaic plant

The PV power plant is situated in a coastal area nearby to the city of Essaouira (Region of Marrakesh-Safi, Morocco) located at 31.52°N, 9.27°W. With average wind speed reaching 7–8 m/s [25]. This area is known as a windy place but has also a reasonably important level of solar irradiation. Its exposure to the Atlantic Ocean moderates the temperature amplitudes compared to inland regions. The meteorological station is installed on the roof of the technical room, located approximately 5 m to the south of the PV plant. All the PV modules are mounted on a galvanized steel support with an inclination of 35° and are oriented to the south, as shown in Fig. 1 (A & B).

The PV field is composed of 32 monocrystalline silicon panels with a peak power of 225 W_p (1559 × 798 × 46 mm with 72 solar cells) from Sun-power (SPR-225-WHT) covered with a 3.2 mm-thick tempered glass and a back polymer sheet.

2.2. Monitoring system

The PV power plant and its meteorological station are fitted up with several sensors to monitor irradiance, wind speed as well as ambient and module temperatures. The monitoring of this PV plant provides useful information about the PV system. With a 5 min time step, the meteorological parameters are recorded by a Sunny Boy Control Plus (SMA) data logger which communicates with the Sunny Sensor Box (SMA) to record the data (see Fig. 1 A & B):

- incident irradiation on a reference cell,
- ambient temperature,
- module temperature provided by a Pt100 sensor installed in the back of one of the PV modules,
- wind speed measured by an anemometer installed at 3 m above the ground just near this PV module.

3. Theoretical models

3.1. PV module temperature calculation models

In addition to the solar radiation, the performance of a PV module depends on its temperature. The latter is determined by an energy balance on a unit area where the absorbed solar energy that is not converted into electricity ([(τα)-η_{PV}]. Gg) is transformed into heat, which is in part dissipated to the surroundings ($U_L(T_m-T_a)$), as shown in Fig. 2. As the PV module efficiency depends essentially on the solar irradiance and the cell temperature [[26–30]], the following hypothesis are assumed for our calculations:

- Layers parallel to the plane of area are isothermal [1] and under steady-state conditions.
- Environment of the PV module is always at ambient temperature.
- Wind speed and direction are assumed to be the same on all the sides of the module.
- Module materials properties are assumed to be independent of temperature, of the incident solar radiation wavelength and angle of incidence.
- Transmittance-absorptance product is in the range of 0.9 [3,9,14,15,31,32].
- Due to thermal inertia, disturbances caused by wind direction and clouds in transit are random and produce a fluctuation around the stationary model.

The heat loss coefficient, U_L, includes losses by convection and radiation from the front and rear surfaces of the PV module to the environment at ambient temperature. Heat losses are almost equally shared between convection and radiation [33] and U_L is a linear function of wind speed ($U_L = U_{L0} + U_{L1}.v$) [7]. However, King et al. [2] used an exponential behavior with wind.

The energy balance for a PV module is given by:

$$[(\tau\alpha) - \eta_{PV}]G_g = U_L(T_m - T_a) = U_{L0}(T_m - T_a) + U_{L1}v(T_m - T_a) \quad (1)$$

The most known nonlinear model for photovoltaic module efficiency is given by the following equation:

$$\eta_{PV} = \eta_{STC}\left[1 + \beta_{P_{mp}}(T_m - T_{ref})\right]\left[1 + \gamma_{P_{mp}} Ln\left(\frac{G_g}{G_0}\right)\right] \quad (2)$$

Where η_{STC} and β_{Pmp} are the module efficiency and the temperature coefficient of maximum power, respectively, at Standard Test Conditions (18.1% and −0.39%/°C, respectively, are given by the manufacturer of m-Si SPR-225-WHT modules). T_{ref} and G_0 are the reference temperature and reference solar irradiance (25 °C and 1000 W/m^2, respectively). γ_{Pmp} is a dimensionless coefficient which is between 0.03 and 0.12 for single crystalline silicon [26–30], and we choose 0.04 in this study.

The steady-state energy balance leads to the following module temperature Tm, based on solar irradiance, ambient temperature and wind speed:

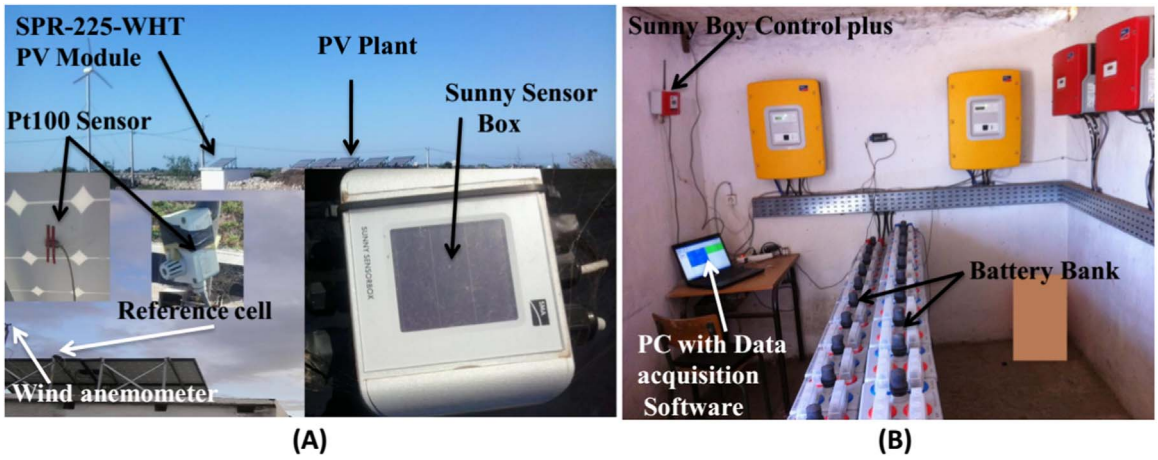

Fig. 1. (A) Outdoor experimental setup, (B) Indoor experimental setup.

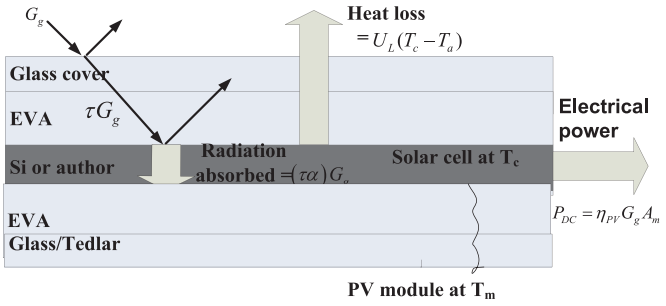

Fig. 2. Energy balance for a PV module.

$$T_m = \frac{U_L T_a + \left[(\tau\alpha) - \eta_{STC}\left(1 - \beta_{P_{mp}} T_{ref}\right)\left(1 + \gamma_{P_{mp}} Ln\left(\frac{G_g}{G_0}\right)\right)\right] G_g}{U_L + \eta_{STC}\beta_{P_{mp}}\left(1 + \gamma_{P_{mp}} Ln\left(\frac{G_g}{G_0}\right)\right) G_g} \quad (3)$$

Another empirical model similar to that of Lasnier [32], which is useful to calculate PV module temperature when the wind data are not available. It is used in this work and is given by:

$$T_m = T_{ref} + C_1(G_g - G_{200}) + C_2(T_a - T_{a,NOCT}) \quad (4)$$

Where T_{ref} is still the reference temperature while $T_{a,NOCT}$ is the ambient temperature considered for NOCT conditions (25 °C and 20 °C, respectively) and G_{200} is the solar irradiance of 200 W/m^2.

Back-surface module and cell temperatures become significantly different for high solar radiation intensities. They can be related by a simple relationship given in Eq. (5), based on the assumption of one-dimensional thermal heat conduction through the encapsulating materials behind the PV cell in the Sunpower SPR 225 WHT. Like most of modules, it is encapsulated by a thin layer of ethylene vinyl acetate (EVA) and Tedlar® back sheet. This temperature difference was evaluated by King et al. [2] to be about $\Delta T = 3°C$ at an irradiance level of $G_0 = 1000$ W/m^2. The module temperature is then given by:

$$T_m = T_c - \frac{G_g}{G_0}\Delta T_0 \quad (5)$$

In the literature, there are several relevant correlations which describe the behavior of PV module or cell temperature (see Table 1). They are based on:

- material properties and PV cell/module construction.
- heat transfer coefficients.
- weather data.

3.2. Statistical data cleaning method

3.2.1. PV module thermal mass

As mentioned above, the thermal mass is among the reasons which may alter temperature measurements and cause noise in the comparison between stationary temperature models and experiments.

The 16th of April 2016, between 12:13 and 12:43 solar time, we exposed abruptly a solar module to the sunshine (30° tilt angle facing south). During the half an hour long exposure, as shown in Fig. 3:

- solar radiation intensity declined slightly from 1034 to 917 W/m^2 with an average of 987 W/m^2; this was expected, given the time shortly after solar noon;
- the ambient temperature was almost constant at 26.5 °C;
- the temperature measured on the module back cover raised with an exponential law from ambient towards a stable value of 49.5 °C with a time constant τ of 8 min. Under these conditions, 18.5 min might be needed to achieve 90% of the steady state value.

Because such a response time of the PV module temperature is due to its significant thermal mass, operating temperature steady state models cannot be fully justified during periods of rapidly changing conditions (like solar radiation intensity during semi-cloudy days). Therefore, it is of interest to determine the thermal response time of the PV module. Previous attempts were made to measure this parameter using indoor measurements and controlling the wind flow over the surface of the panel with fans. Actual PV module temperature is driven by ambient temperature variations but also by fluctuating wind speeds and directions, quite difficult to reproduce in indoor experiments.

3.2.2. Comparison of experimental module temperatures with theoretical models

Data were recorded with a 5-min step, between 25 April 2011 and 02 of November 2011, during the first year of the PV plant operation (see Fig. 4). After removal of nighttime records, 6123 data sets remain.

We compare the measured PV module temperature, namely $T_{m,meas}$, with the calculated ones, $T_{m,calcul}$, for each of the theoretical models listed in Table 1. In order to simplify the analysis, we assume that the PV module efficiency is equal to the reference efficiency (STC), as done by other authors [1,9,13–15,25,26,33]. Therefore, Eq. (1), becomes:

$$[(\tau\alpha) - \eta_{STC}]G_g = U_{L0}(T_m - T_a) + U_{L1}v(T_m - T_a) \quad (16)$$

For the models which give directly the cell temperature, we have included a correction taking into account the thermal heat conduction through the encapsulating materials behind the PV cells of Eq. (5). For each comparison, we calculated:

Table 1
PV cell/module temperature (°C) as a function of weather data and empirical parameters.

Correlations	Equations	Comments	Ref.
$T_c = T_a + \frac{G_g}{800}(T_{NOCT} - 20)$	Eq. (6)	**NOCT** used in this study is 45 °C	[11]
$T_c = T_a + \frac{G_g(T_{NOCT}-20)}{800}\left[1 - \frac{\eta_{STC}}{(\tau\alpha)}\right]\frac{9.5}{5.7+3.8v}$	Eq. (7)	**NOCT Dyn 1**, use the correlation 1 of McAdams for convection	[14,34]
$T_c = T_a + \frac{G_g(T_{NOCT}-20)}{800}\left[1 - \frac{\eta_{STC}}{(\tau\alpha)}\right]\frac{8.5}{5.7+2.8v}$	Eq. (8)	**NOCT Dyn 2**, use the correlation 1 of Skoplaki for the convection	[15]
$T_c = T_a + \frac{G_g(T_{NOCT}-20)}{800}\left[1 - \frac{\eta_{STC}\left(1-\beta P_{mp}T_{ref}\right)}{(\tau\alpha)}\right]\frac{9.8}{6.5+3.3v}$	Eq. (9)	**Skoplaki 1**, use the correlation 2 of Skoplaki for the convection	[15]
$T_c = 30 + 0.0175(G_g - 300) + 1.14(T_a - 25)$	Eq. (10)	**Lasnier 1**, for p-Si	[32]
$T_c = T_a + k_{\Delta T} G_g$	Eq. (11)	**Skoplaki2**, with $k_{\Delta T} = 0.02 - 0.04K.\ m^2/W$	[35]
$T_c = T_a + \frac{\left[1-\eta_{PVSyst}\right](\tau\alpha)G_g}{U_{L0}+U_{L1}v}$	Eq. (12)	**PVSyst**, $\eta_{PVSyst} = 0.1$, $U_{L0} = 29$ W/m²/°C and $U_{L1} = 0$ W s/m³/°C	[38,39]
$T_c = \frac{U_L T_a + \left[(\tau\alpha) - \eta_{STC}\left(1-\beta_{Pmp}T_{ref}\right)\right]G_g}{U_L + \eta_{STC}\beta_{Pmp}G_g}$	Eq. (13)	**Mattei**, uses $(\tau\alpha) = 0.81$ and $U_L = 26.6 + 2.3$ v	[1]
$T_m = T_a + \frac{S}{U_{L0}+U_{L1}v}$	Eq. (14)	**Faiman**, use $S = (\tau\alpha)G_g$, $U_{L0} = 30.02$ W/m²/°C and $U_{L1} = 6.28$ W s/m³/°C	[7,16]
$T_m = T_a + G_g b e^{(a+bv)}$	Eq. (15)	**King** (Sandia), with a = −3.56 and b = −0.075 s/m	[2,38]

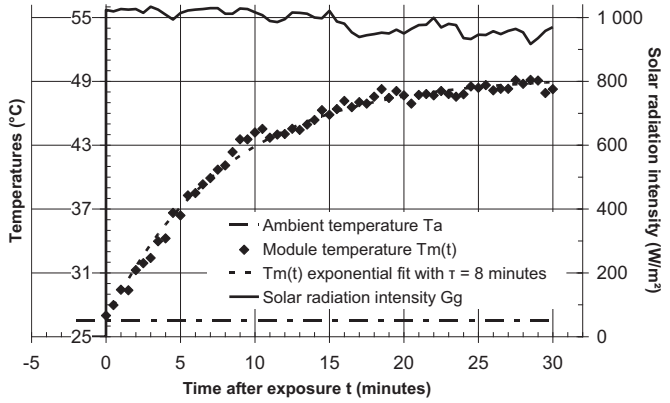

Fig. 3. Temperature vs. time with thermal mass.

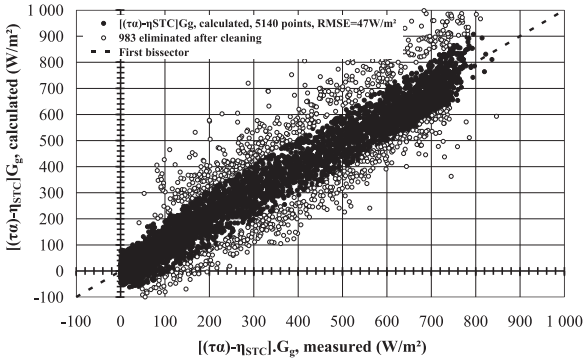

Fig. 4. The plot of [(τα)-ηSTC]Gg calculated with Eq. (16) versus measured for all 6123 experimental data. The 5140 solid circles are proper data measured. The 983 open circles are points eliminated after the cleaning described in the text. The straight line represents the ideal straight with slope 1 (First bisector).

- the linear coefficient of correlation (R^2), used for a global evaluation of the model,
- the root mean squared error (RMSE), used to evaluate the fluctuations around the model itself, and use them as reliability quantitative indicators of each model.

Obviously, the best models are the ones where the linear regression of $T_{m,calcul}$ versus $T_{m,meas}$ matches as perfectly as possible the first bisector, thus which maximize R^2 and minimize RMSE.

3.2.3. Data cleaning method

The scope of this part is to eliminate from the data sets those which might content errors caused by spurious or transient effects (from wind direction, from scattered clouds, from accidental shading…) delayed by the thermal mass.

As $[(\tau\alpha)-\eta_{STC}].Gg$ is a bilinear function of the two variables (T_m-T_a) and $v.(T_m-T_a)$. A bilinear regression analysis by the mean least squares method allows to calculate an approximate value of the coefficients U_{L0} and U_{L1} as well as the straight line fit $[U_{L0} + U_{L1}.\ v].(T_m-T_a)$ which is in fact the average calculated value of $[(\tau\alpha)-\eta_{STC}].Gg$.

The calculated average $[(\tau\alpha)-\eta_{STC}].Gg$ is plotted against its actual values in Fig. 4 and the RMSE is calculated. This Figure shows that it is acceptable to model the temperature.

Fig. 4 shows one of the visual aspects of the cleaning where 983 points are removed from 6140. If the distribution of the points around the average is supposed to have a single Gaussian distribution, there will be around 2% of the data sets outside the interval [average − 2.327 × RMSE, average + 2.327 × RMSE]. All the data sets outside this interval are removed, the new average and RMSE are calculated and the data sets outside the new interval [average − 2327.RMSE, average + 2327.RMSE] removed again. The operation is repeated until there are no more data sets outside the interval Fig. 5(A) shows the effect of our cleaning which has removed the two bumps above and below the average. Apart from spurious points which might be in the peripheral area, these two bumps can be interpreted in terms of dynamic effects when increasing or decreasing abruptly the incident solar radiation intensity, with thermal inertia involved.

If the distribution of data around the average was "perfectly Gaussian", the cleaning would have been useless and this would have resulted in:

- a percentage of removed points around 2%,
- and an RMSE almost unchanged if not increased.

Instead of this, we note that rejecting data from the peripheral zone (outside the average ± 2.327.RMSE) was useful and efficient since, after cleaning the 6123 data sets:

- 16% have been removed (only 5140 kept),
- and RMSE decreased to almost half of its initial value from around 81 W/m² to around 48 W/m² (and correlation coefficient increased from 96.1% to 98.59%).

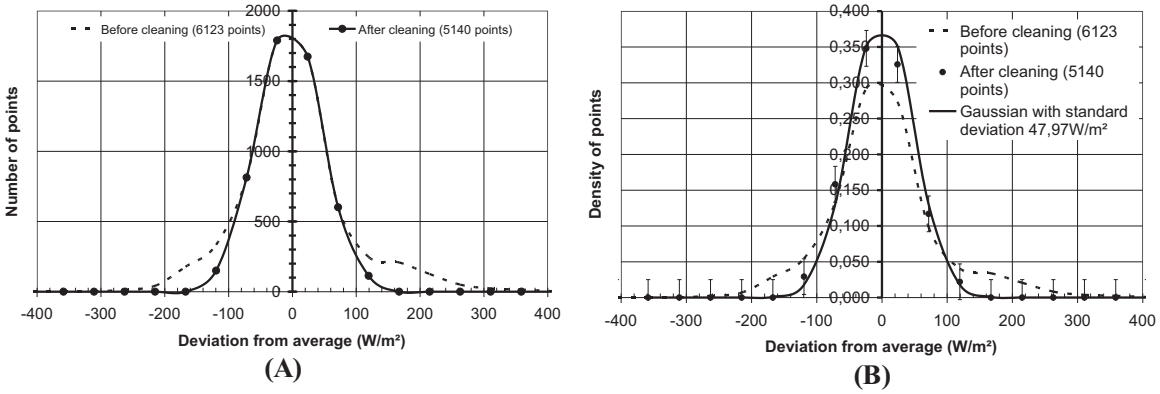

Fig. 5. Number (A), density (B) and Gaussian fit of points of Fig. 3 before/after cleaning.

Table 2
Values of empirical parameters and statistical coefficients for our models with/without wind.

Proposed model	Data sets [cleaning]	U_{L0} [W/ (m^2 °C)]	U_{L1} [W.s/ (m^3°C)]	C_1 [°C/ (Wm^2)]	C_2	RMSE	R^2 [%]
With wind	6123 (before)	27.58 ± 0.27	4.69 ± 0.07	– – –	– – –	81.41 W/m^2	96.10
Eq. (16)	5140 (after)	24.99 ± 0.19	5.93 ± 0.05	– – –	– – –	47.97 W/m^2	98.59
Without wind	5140 (before)	– – –	– – –	0.0126 ± 0.0001	1.03 ± 0.01	2.33 °C	91.68
Eq. (4)	5077 (after)	– – –	– – –	0.0123 ± 0.0001	1.04 ± 0.01	2.24 °C	92. 08

The RMSE being theoretically inversely proportional to the square root of the data sample size, this means that we have improved the global fluctuation of the distribution and, at the same time, the quality of the data sample.

All that remains is to justify a posteriori the Gaussian distribution of the points around the average, as we have presupposed. Fig. 5(B) shows the normalized density of points before and after cleaning and a Gaussian distribution theoretically calculated with the same standard deviation than our RMSE.

Fig. 5(B) clearly shows:

- that the hypothesis of a Gaussian distribution around the average is confirmed with an absolute precision of ± 0.025 in density,
- how the precision has been improved by sharpening the density of points around the average.

At the bottom line, we could increase fairly the response to noise ratio.

During the two last years, we have intensively and successfully used the same method to clean other type of data but the choice of 2.327 RMSE, and its related 98% of the Gaussian distribution data, can be changed but, of course, after:

- adopting an appropriate model to the specific case,
- taking into consideration the related experimental conditions.

4. Models validation

4.1. Data evaluation

In our data sets, for which irradiance was always below 1200 W/m^2:

- ambient temperature was between 12.4 °C and 37.5 °C with an average of 21 °C,
- module temperature was between 11.8 °C and 48 °C with an average of 28.6 °C, and varied up to 25 °C above the ambient temperature. This reasonably low heating is due to the wind cooling effect on the encapsulated solar cells. It can be explained by the wind speed levels observed in Elkaria village where wind speed was between 0 and 13.5 m/s with an average of 3.3 m/s.

4.2. Proposed models with or without using wind data

Among the models found in the literature (see Table 1), four of them [1,7,14,15] have studied the increase in module temperature above the ambient temperature as a linear function of irradiance with a slope itself linear to wind speed. Equation (6), allows to calculate the solar radiation absorbed by the encapsulated solar cells but not converted into electricity and which heats them above ambient.

In fact, the linear regression analysis of Fig. 4 using Eq. (16), gives 2 different values (Table 2):

- U_{L0} = 27.58 W/m^2 °C and U_{L1} = 4.69 W s/m^3/°C before data cleaning,
- U_{L0} = 24.99 W/m^2 °C and U_{L1} = 5.93 W s/m^3/°C after data cleaning.

Even the standard deviation on these values is reduced after data cleaning:

- from 0.27 to 0.19 W/m^2 °C for U_{L0},
- from 0.07 to 0.05 W s/m^3/°C for U_{L1}.

When wind is neglected, using Eq. (4) as a model and applying the above method of data cleaning allows also to find the empirical parameters C_1 and C_2. As shown in Table 2, an additional cleaning of the 5140 data sets removed only 63 of them (about 1.2%), and did not lead to substantial improvements neither in the root mean square error (RMSE), nor in the correlation coefficient (R^2). The major result to remember here is that the error on the module temperature lies around 2.24 − 2.33 °C for this model.

4.3. Parametric identification of our two thermal models

By using Eq. (1) with Eq. (2), the left term of $[(\tau\alpha)\text{-}\eta PV]G_g/(T_m\text{-}T_a) = U_L = U_{L1}.v + U_{L0}$ is calculated for all kept 5140 data. Fig. 6 shows a plot of $[(\tau\alpha)\text{-}\eta_{PV}]G_g/(T_m\text{-}T_a)$ against wind speed for 3773 experimental points obtained after the same cleaning described in the text above.

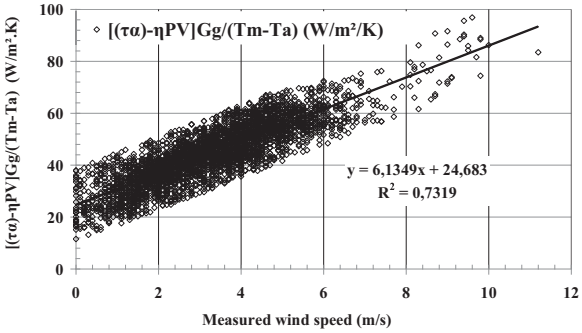

Fig. 6. The plot of [(τα)-ηPV]Gg/(Tm-Ta) versus measured wind speed v, and associated least squares linear fit to the data, for all 3773 experimental points after cleaning.

From the least-squares fit of the data ($R^2 = 0.73$), we determine the two heat loss coefficient elements (U_{L0} and U_{L1}) in a more conventional way:

- the Y-intercept value gives $U_{L0} = 24.68$ W/m^2/°C,
- the slope value gives $U_{L1} = 6.13$ W s/m^3/°C.

These values are very close to the former ones used with the assumption, $\eta_{PV} = \eta_{STC}$, ($U_{L0} = 24.99$ W/m^2 °C and $U_{L1} = 5.93$ W s/m^3/°C). Also, this results shows that it is possible to overlook the temperature dependence of η_{PV} in PV module temperature calculation, such as in Faiman model (Eq.X).

It should be noted that the determined coefficients are influenced by the location of the site, the height where the wind speed/direction is measured, the mounting structures and the module materials. These effects may account for the various values reported in the literature:

- $U_{L0} = 26.6$ W/(m^2°C) and $U_{L1} = 2.3$ W s/(m3°C) for Mattei et al. [1],
- $U_{L0} = 25.0$ W/(m^2°C) and $U_{L1} = 6.84$ W s/(m^3°C) for Faiman et al. [7],
- $U_{L0} = 30.02$ W/(m^2°C) and $U_{L1} = 6.28$ W s/(m3°C) for Koehl et al. [16],
- $U_{L0} = 25.3$ W/(m^2°C) and $U_{L1} = 6.0$ W s/(m3°C) for Bardhi et al. [3],
- $U_{L0} = 29$ W/(m2°C) and $U_{L1} = 0$ W s/(m3°C) for PVsyst [37,39],
- $U_{L0} = 20$ W/(m2°C) and $U_{L1} = 6$ W s/(m3°C) obtained by Kaldellis et al. [39] with local data,
- $U_{L0} = 25$ W/(m2°C) and $U_{L1} = 1.2$ W s/(m3°C) obtained by the last author with standard "meteo" data such as those in the "US TMY2″.

Despite the fact that the simplicity of the NOCT-based model using Eq. (6) [11] is subject to some criticism it gives a reasonable value $U_L = 32.0$ W/m^2/°C for its specific conditions since, at 1 m/s:

- $U_L = 30.82$ W/m^2/°C is found with our two elements (U_{L0} and U_{L1}) of the heat transfer coefficient,
- $U_L = 28.9$ W/m^2/°C is found with Mattei et al. [1] ones,
- $U_L = 31.84$ W/m^2/°C is found with Faiman et al. [7] ones,
- $U_L = 28.6$ W/m^2/°C is found with Jones [22] ones.

For the thermal models without wind:

- $C_1 = 0.0175$ °C/W/m^2 and $C_2 = 1.14$ was found by Lasnier et al. [32],
- $C_1 = 0.0123$ °C/W/m^2 and $C_2 = 1.04$ found for this work which are in an acceptable agreement with the former values.

5. Results and discussion

5.1. Calculation procedure

By using all measured and recorded data during the study period, *before* and *after* data cleaning, we calculate $T_{m,calcul}$ by applying the ten models and compare them with their corresponding measured values $T_{m,meas}$, only *after* data cleaning for two cases:

- models without wind are shown in Fig. 7 (A1, A2, A3, A4),
- models with wind are shown in Fig. 7 (B1, B2, B3, B4, B5, B6).

The calculated values of the statistical coefficients (R^2 and RMSE) *before* and *after* data cleaning are listed in Table 3. The comparison of the eight models *after* cleaning with those *before* cleaning shows:

- a slight increase of the correlation coefficient R^2 values,
- a significant decrease of the RMSE.

The values in bold are associated to the accurate model which maximize R^2 and minimize RMSE for both cases (with/without wind).

Fig. 8 shows a plot of the RMSE against the correlation coefficients R^2 obtained for all the previously mentioned models (5140 points after cleaning). The best models fall in the neighborhood of the "center of the target" constituted by the ideal model reliability indicators ($R^2 = 100\%$, RMSE = 0). R^2 is used to evaluate the linearity of the difference between calculation and measurement while the RMSE quantifies the fluctuations around the model. Their values are found to show a good agreement between $T_{m,meas}$ and $T_{m,calcul}$, for all models,

- the (1-R^2) parameter was found to be in the range of [1.2–6.0]%,
- with a RMSE in the range of [1.1–3.9] °C.

These last values are satisfactory in the extent to validate the ten models (including ours) in this site for this long experiment.

5.2. Models comparison

As cited above, firstly, we compared $T_{m,meas}$ and $T_{m,calcul}$, as shown in Fig. 7; the NOCT Eq. (7) (A1) [11], PVSyst Eq. (12) (A2) [37], Sandia Eq. (15) (B1) [2], NOCT Dyn1 Eq. (7) (B2) [14] and Faiman Eq. (14) (B5) [7] models:

- overestimate the PV module temperature for high irradiance values with a difference of 2–10 °C,
- underestimate it at low irradiance with a difference of 1–2 °C.

The Lasnier 1 Eq. (10) (A3) [32], Mattei Eq. (13) (B3) [1] and NOCT Dyn2 Eq. (8) (B4) [15] models as well ours without wind Eq. (4) (A4):

- underestimate this temperature for high irradiance with a difference of 2–4 °C,
- overestimate it at low irradiance with a difference of 1 °C.

Secondly, we studied and compared all models with/without wind, as shown in Fig. 8. After this comparison, based on the couple (R^2 and RMSE), we see that the models that include the wind speed perform significantly better than the others ignoring the wind effect. So, according to our results, the inclusion of the wind data if it is available plays an important role in the PV module temperature calculation.

5.2.1. Models without wind

By comparing only the models without wind, as shown in Fig. 7 (A1, A2, A3, and A4), it's observed that:

- the NOCT Eq. (6) (A1) [11] and PVSyst Eq. (12) (A2) [37] models overestimate the PV module temperature,
- the Lasnier 1 Eq. (10) [32] model and ours described in Eq. (4) slightly underestimate it.

However the models in which the wind is not considered does not

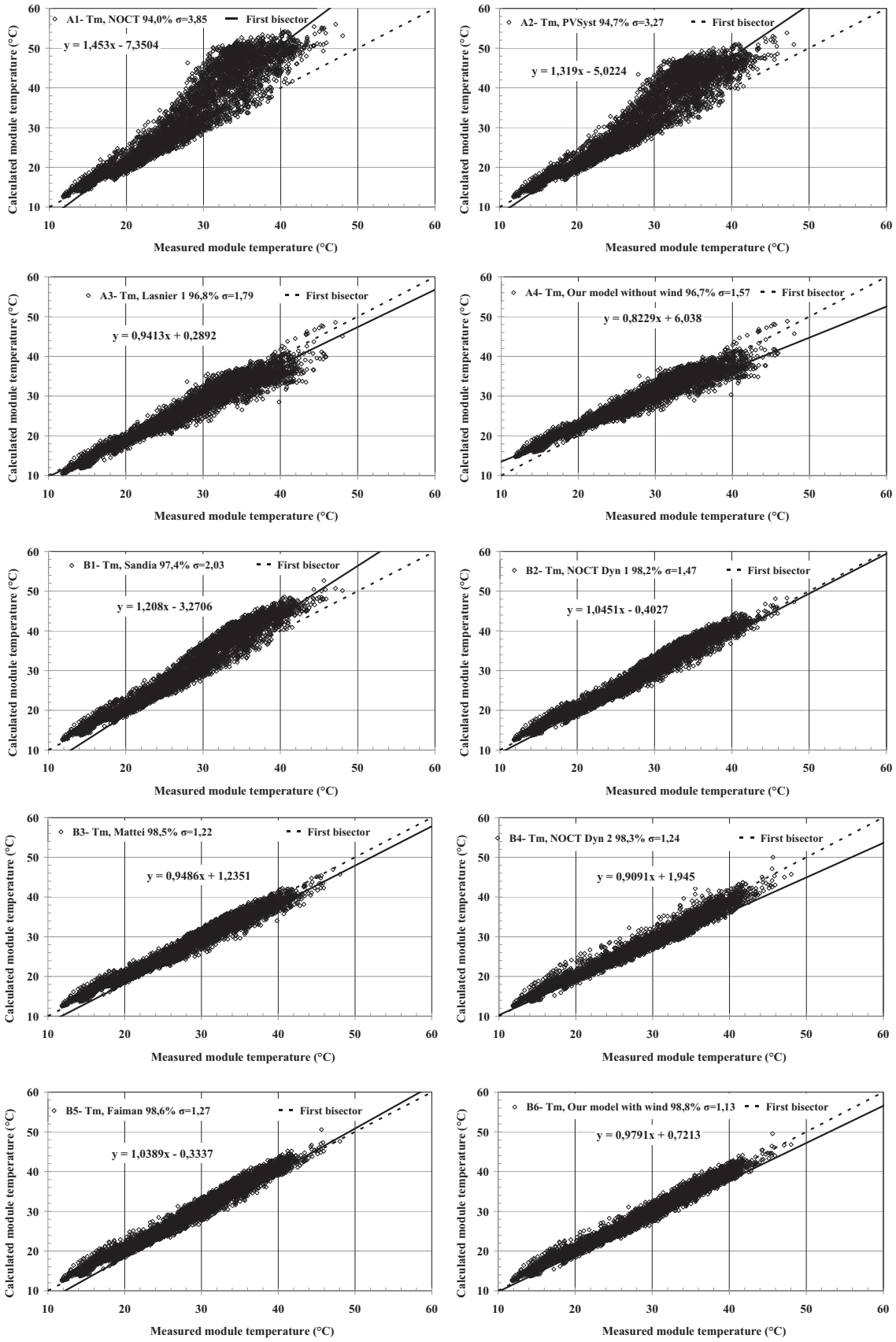

Fig. 7. The models without wind (A1, A2, A3, A4) and with wind (B1, B2, B3, B4, B5, B6) calculated vs. the measured module temperatures after cleaning. The dashed line represents the true linear regression fits and the straight line represents the ideal straight with slope 1 (First bisector).

Table 3
The statistical coefficients (R^2 and RMSE) of all models with/without wind speed vs. experimental measurements temperature before and after cleaning.

Number of Data sets			6123 points before cleaning		5140 points after cleaning	
Group	Model	Equations	R^2 (%)	RMSE (°C)	R^2 (%)	RMSE (°C)
A-No wind considered in model	A1- Tm, NOCT	Eq. (6)	91.80	4.46	93.97	3.85
	A2- Tm, PVSyst	Eq. (12)	92.44	3.87	94.66	3.27
	A3- Tm, Lasnier 1	Eq. (10)	**94.43**	**2.35**	**96.76**	1.79
	A4- Tm, Our model without wind	Eq. (4)	–	–	96.73	**1.57**
B-Wind considered in model	B1- Tm, Sandia (King)	Eq. (15)	95.39	2.63	97.44	2.03
	B2- Tm, NOCT Dyn 1	Eq. (7)	95,85	2.21	98.18	1.47
	B3- Tm, Mattei	Eq. (13)	96.12	1.94	98.47	1.22
	B4- Tm, NOCT Dyn 2	Eq. (8)	95.60	**1.92**	98.30	1.24
	B5- Tm, Faiman	Eq. (14)	**96.37**	1.99	98.61	1.27
	B6- Tm, Our model with wind	Eq. (3)	–	–	**98.77**	**1.13**

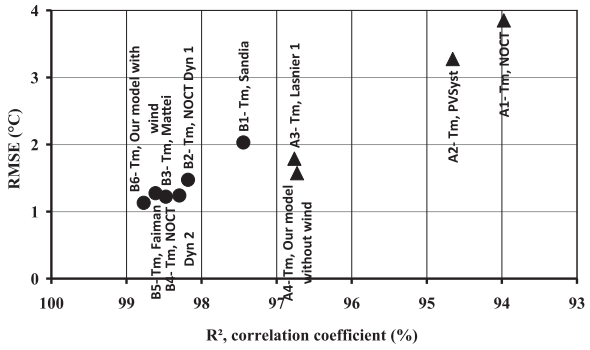

Fig. 8. Scatter plots of R^2 and RMSE (°C) obtained comparing the relation between measured and calculated PV module temperature after cleaning.

represent a good correlations to calculate the module temperature, this is due to the fact that the RMSE is in the range of [2–4] °C and the R^2 is between [94 − 97]%, while, as it can be seen in Fig. 7, the Lasnier 1 model Eq. (10) [13] and ours in Eq. (4) perform better than the others, and give better simulations among the models ignoring the wind (Eq. (6) and Eq. (10)).

5.2.2. Models with wind

As shown in Fig. 7 (B1, B2, B3, B4, B5, B6),

- NOCT Dyn 1 Eq. (7) [14], Faiman Eq. (14) [7] and Sandia Eq. (15) [2] models overestimate the module temperature,
- those of Mattei Eq. (13) [1] and NOCT Dyn 2 Eq. (8) [15] underestimate it,
- our model described in Eq. (3) calculates the module temperature with a good accuracy, and the linear regression is quasi-confounded with the first bisector in this case.

Consequently, in order to calculate the module temperature, the models with wind are suitable and yield the best results compared to those without wind, as depicted in Fig. 8, since:

- the RMSE is between [1,2] °C,
- the R^2 is in the range of [97 − 99]%.

From Table 3 and Fig. 8, we see that among all tested models,

- our proposed model with wind in Eq. (3) is the most accurate model where R^2 is 98.77% with a RMSE of 1.12 °C,
- the NOCT model Eq. (6) [11] is the least accurate, this later overestimates the PV module temperature with a RMSE of 3.9 °C, due to the fact of not considering the wind effect in this model,
- our proposed model without wind Eq. (4), can be used when the wind data is not available, although the accuracy is less satisfactory, with a RMSE of 1.7 °C and R^2 of 96,7%.

It should be noted that,

- the Faiman model Eq. (14) [7] gives good results, despite the underestimation of absorbed solar radiation,
- the thermal mass and the wind direction are not considered in this study, if these parameters are taken into account, the model will be more accurate, where the R^2 and RMSE, will approach 100% and 0 °C, respectively.

In the case of Elkaria village, the high values of wind speed minimized the thermal mass of the PV module and the weather data are recorded with a 5-min time step.

More dispersion is observed for the high intensity of solar radiation, when we plot the daytime curves, as it is illustrated in Fig. 7 and in Table 3. However, when considering the temperature difference, due to the thermal resistance between the cell and the back of the module, Eq. (5), the statistical coefficients are only improved by such relation, thus, to increase the accuracy of each model. Moreover, it is suitable to include this temperature difference in all models except Faiman Eq. (14) and Sandia Eq. (15) ones. These results show that the back sheet has an important thermal resistance for the used module in this study.

From this analysis, we deduced that it is difficult to apply a unique formula to calculate accurately the PV module/cell temperature. However, in order to include correctly the wind effect in the PV module temperature calculation model, the U_L should be correlated accurately.

6. Conclusion

In the intent to estimate the energy yield, it is necessary to calculate accurately the photovoltaic module/cell temperature, which affects significantly their electrical efficiency. In this framework, we presented eight theoretical models, and then developed two new models in order to calculate the PV module temperature. These models are validated, evaluated and compared with experimental data. From the presented results, it's observed that there is a satisfactory agreement between the calculated and measured module temperature for the ten models. Eq. (3), can be used to calculate PV module temperature with a high degree of precision. Pair of heat loss coefficients U_{L0} and U_{L1} are determined experimentally as we have illustrated above, these values can be applied in another site. When the wind data is not available, Eq. (4) can be used.

We have done a comparison of the corresponding statistical coefficients (R^2 and RMSE); between calculated and measured PV module temperatures; for all models with/without wind. The results show that the inclusion of the wind parameter and the thermal resistance (between the cells and the rear face of the PV module) makes the module

temperature calculation more accurate.

Using the developed models, various studies can be performed to evaluate the thermal performance of a PV module under different environmental and operating conditions.

Acknowledgements

This work was supported by the Propre.Ma project (Inno'PV 2013) funded by IRESEN, Morocco. The PV plant has been installed in the framework of the HYRESS project funded FP6-INCO (ID: 31994) by the European Union.

References

[1] M. Mattei, G. Notton, C. Cristofari, M. Muselli, P. Poggi, Calculation of the polycrystalline PV module temperature using a simple method of energy balance, Renew. Energy 31 (2006) 553–567, http://dx.doi.org/10.1016/j.renene.2005.03.010.

[2] D.L. King, J.A. Kratochvil, W.E. Boyson, Photovoltaic array performance model Online, 8, 2004, pp. 1-19 doi: 10.2172/919131.

[3] M. Bardhi, G. Grandi, G.M. Tina, Comparison of PV Cell Temperature Estimation by Different Thermal Power Exchange Calculation Methods, in: Proceedings of International Conference on Renewable Energies and Power Quality, ICREPQ 28–10, 2012.

[4] Planning and installing photovoltiac systems: a guide for installers, architects, and engineers, Deutsche Gesellschaft fur Sonnenenergie (DGS), 5th ed., Landesverband Berlin Brandenburg e.V, Berlin. ⟨WWW.epices-energie.fr⟩.

[5] International Electrotechnical Commission 2005. IEC 61215 Ed. 2.0 (English 2005). Crystalline silicon terrestrial photovoltaic (PV) modules – Design qualification and type approval., Ed. 2.0.

[6] J. Kurnik, M. Jankovec, K. Brecl, M. Topic, Outdoor testing of PV module temperature and performance under different mounting and operational conditions, Sol. Energy Mater. Sol. Cells 95 (2011) 373–376, http://dx.doi.org/10.1016/j.solmat.2010.04.022.

[7] D. Faiman, Assessing the outdoor operating temperature of photovoltaic modules, Prog. Photovolt. Res. Appl. 16 (2008) 307–315, http://dx.doi.org/10.1002/pip.

[8] J.K. Tonui, Y. Tripanagnostopoulos, Air-cooled PV/T solar collectors with low cost performance improvements, Sol. Energy 81 (2007) 498–511.

[9] C. Schwingshackl, M. Petitta, J.E. Wagner, G. Belluardo, D. Moser, M. Castelli, M. Zebisch, A. Tetzlaff, Wind effect on PV module temperature: analysis of different techniques for an accurate estimation, Energy Procedia 40 (2013) 77–86, http://dx.doi.org/10.1016/j.egypro.2013.08.010.

[10] M. Oukili, S. Zouggar, M. Seddik, T. Ouchbel, Comparative study of the moroccan power grid reliability in presence of photovoltaic and wind generation, Energy Procedia 2013 (2013) 366–377.

[11] P. Nolay, Ecole des Mines, Sophia-Antipolis, Développement d'une Méthode Générale d'analyse des Systèmes Photovoltaïques, 1987.

[12] M. Muller, B. Marion, J. Rodriguez, Evaluating the IEC 61215 Ed. 3 NMOT procedure against the existing NOCT procedure with PV modules in a side-by-side configuration, in: Proceedings of 38th Photovoltaiic Specialists Conference (PVSC), 2012 IEEE, pp. 697–702. doi:http://dx.doi.org/10.1109/PVSC.2012.6317705.

[13] S.A. Kalogirou, Solar Energy Engineering Processes and Systems, 2nd ed, 2014.

[14] J.A. Duffie, W.A. Beckman, Solar Engineering of Thermal Processes, 3rd ed, 2006.

[15] E. Skoplaki, A.G. Boudouvis, J.A. Palyvos, A simple correlation for the operating temperature of photovoltaic modules of arbitrary mounting, Sol. Energy Mater. Sol. Cells 92 (2008) 1393–1402, http://dx.doi.org/10.1016/j.solmat.2008.05.016.

[16] M. Koehl, M. Heck, S. Wiesmeier, J. Wirth, Modeling of the nominal operating cell temperature based on outdoor weathering, Sol. Energy Mater. Sol. Cells 95 (2011) 1638–1646, http://dx.doi.org/10.1016/j.solmat.2011.01.020.

[17] S. Kurtz, D. Miller, M. Kempe, N. Bosco, K. Whitefield, M.J. Wohlgemuth, N. Dhere, T. Zgonena, Evaluation of High-Temperature Exposure of Photovoltaic Modules: Preprint. ⟨http://www.osti.gov/bridge⟩.

[18] J.C. Sánchez Barroso, N. Barth, J.P.M. Correia, S. Ahzi, M.A. Khaleel, A computational analysis of coupled thermal and electrical behavior of PV panels, Sol. Energy Mater. Sol. Cells 148 (2016) 73–86, http://dx.doi.org/10.1016/j.solmat.2015.09.004.

[19] S. Armstrong, W.G. Hurley, A thermal model for photovoltaic panels under varying atmospheric conditions, Appl. Therm. Eng. 30 (2010) 1488–1495, http://dx.doi.org/10.1016/j.applthermaleng.2010.03.012.

[20] G. Notton, C. Cristofari, M. Mattei, P. Poggi, Modelling of a double-glass photovoltaic module using finite differences, Appl. Therm. Eng. 25 (2005) 2854–2877.

[21] D.L. King, J.K. Dudley, J.A. Kratochvil, W.E. Boyson, Temperature coefficients for PV modules and arrays: measurements methods, difficulties, and results, in: Proceedings of 25th IEEE Photovoltaic Specialists Conference, 1997, pp. 1183–1186.

[22] A.D. Jones, C.P. Underwood, A thermal model for photovoltaic systems, Sol. Energy 70 (2001) 349–359, http://dx.doi.org/10.1016/S0038-092X(00)00149-3.

[23] S.J. Ransome, P. Funtan, Why hourly averaged measurement data is insufficient to model PV system performance accurately, in: Proceedings of 20th European Photovoltaic Solar Energy Conference: 2005: pp. 2752–2755.

[24] Moroccan Agency of Solar Energy (MASEN). ⟨www.masen.org.ma/⟩.

[25] A. El Fathi, L. Nkhaili, A. Bennouna, A. Outzourhit, Performance parameters of a standalone PV plant, Energy Convers. Manag. 86 (2014) 490–495, http://dx.doi.org/10.1016/j.enconman.2014.05.045.

[26] D.L. Evans, Simplified method for predicting photovoltaic array output, Sol. Energy 27 (1981) 555–560, http://dx.doi.org/10.1016/0038-092X(81)90051-7.

[27] S. R. Williams, T.R. Betts, T. Helf, R. Gottschalg, H.G. Beyer, D.G. Infield, Modelling long-term module performance based on realistic reporting conditions with consideration to spectral effects, in: Proceedings of the 3rd World Conference Photovoltaic Energy Conversion: 2003, pp. 1908–1911.

[28] G. Notton, V. Lazarov, L. Stoyanov, Optimal sizing of a grid-connected PV system for various PV module technologies and inclinations, inverter efficiency characteristics and locations, Renew. Energy 35 (2010) 541–554, http://dx.doi.org/10.1016/j.renene.2009.07.013.

[29] F. Fouladi, P. Henshaw, D.S.-K. Ting, Enhancing smart grid realisation with accurate prediction of photovoltaic performance based on weather forecast, Int. J. Environ. Stud. 70 (2013) 754–764, http://dx.doi.org/10.1080/00207233.2013.798497.

[30] E. Kaplani, S. Kaplanis, Thermal modelling and experimental assessment of the dependence of PV module temperature on wind velocity and direction, module orientation and inclination, Sol. Energy 107 (2014) 443–460, http://dx.doi.org/10.1016/j.solener.2014.05.037.

[31] E. Skoplaki, J.A. Palyvos, On the temperature dependence of photovoltaic module electrical performance: a review of efficiency/power correlations, Sol. Energy 83 (2009) 614–624, http://dx.doi.org/10.1016/j.solener.2008.10.008.

[32] S. Kalogirou, Copyright, Elsevier Inc., doi:http://dx.doi.org/10.1016/B978-0-12-374501-9.00014-5.

[33] M. Bardhi, G. Grandi, M. Premuda, Steady-State Global Power Balance for Ground-Mounted Photovoltaic Modules, 2011, pp. 359–365.

[34] M. WC, Heat transmission, 3rd ed., New York, 1954.

[35] E. Skoplaki, J.A. Palyvos, Operating temperature of photovoltaic modules: a survey of pertinent correlations, Renew. Energy 34 (2009) 23–29, http://dx.doi.org/10.1016/j.renene.2008.04.009.

[36] Website of PVSyst. ⟨http://www.pvsyst.com/en/⟩ (accessed 11 August 2016).

[37] Website of Sandia National Laboratory (SNL) to Improve PV Performance Modeling Collaborative (PVPMC). ⟨https://pvpmc.sandia.gov/modeling-steps/2-dc-module-iv/cell-temperature/pvsyst-cell-temperature-model/⟩ (accessed 11 August 2016), 2016.

[38] Website of Sandia National Laboratory (SNL) to Improve PV Performance Modeling Collaborative (PVPMC1). ⟨https://pvpmc.sandia.gov/modeling-steps/2-dc-module-iv/module-temperature/sandia-module-temperature-model/⟩ (accessed 11 August 2016), 2016.

[39] J.K. Kaldellis, M. Kapsali, K.A. Kavadias, Temperature and wind speed impact on the efficiency of PV installations. Experience obtained from outdoor measurements in Greece, Renew. Energy 66 (2014) 612–624, http://dx.doi.org/10.1016/j.renene.2013.12.041.